

Guadalupian (Middle Permian) $\delta^{13}\text{C}_{\text{org}}$ changes in the Lower Yangtze, South China

Hengye Wei^{1,2}  · Ziao Geng² · Xuan Zhang²

Received: 24 October 2019 / Revised: 14 March 2020 / Accepted: 13 April 2020 / Published online: 23 April 2020
© Science Press and Institute of Geochemistry, CAS and Springer-Verlag GmbH Germany, part of Springer Nature 2020

Abstract The Middle Permian Guadalupian witnessed significant environmental changes in the Phanerozoic such as large-scale sea-level drop, supercontinent Pangaea assembly, and transition from Early Permian glaciation to Late Permian non-glacial intervals. Carbon-isotope tracers can provide insights for these environmental changes. The $\delta^{13}\text{C}$ studies of the entire Guadalupian epoch are rare, and most of them have focused on near the end of Guadalupian and carbon isotopes of inorganics. Here, we present carbon isotopic compositions of organic matters in the Guadalupian from two sections (Chaohu and Xiaolao) in the Lower Yangtze area, South China. Our results show that $\delta^{13}\text{C}_{\text{org}}$ profiles in the Guadalupian show a peak in the Roadian and a gradual negative shift from the Roadian to the middle Capitanian. These trends can be matched by $\delta^{13}\text{C}$ changes of carbonate rocks or organic matter in South China and other places in the world, representing a global carbon cycle signal. The Roadian positive peak was probably due to high productivity which was caused by upwelling during cooling time. The gradual negative shift of $\delta^{13}\text{C}$ was caused mainly by a decrease of organic matter burial on land and in the ocean, resulting from global sea-level drop and anoxia-caused benthos decline, respectively. The less important causes for the gradual $\delta^{13}\text{C}$ negative shift are volcanic-gases releasing, decreased mountain belts, and the resultant reduced silicate weathering-consumption of CO_2 . The gradual negative shift of $\delta^{13}\text{C}$ coincides with the

gradual extinction in the Guadalupian. Therefore, global sea-level drop and marine reducing conditions may be the main causes of the gradual extinction in the Guadalupian.

Keywords Organic-carbon isotope · Carbon cycle · Mass extinction · Kuhfeng Formation · Chaohu · Xiaolao

1 Introduction

The Middle Permian Guadalupian epoch was a transition time from Early Permian glacial interval to Late Permian non-glacial interval (Veevers and Powell 1987). Associated with this environmental change, a significant mass extinction occurred from the mid-Capitanian to the Guadalupian–Lopingian (G–L) boundary (Shen and Shi 2009; Bond et al. 2010a). This mass extinction is called Guadalupian mass extinction (Clapham 2015), and also called end-Guadalupian (Jin et al. 1994; Shen and Shi 1996, 2002) or mid-Capitanian mass extinction (Bond et al. 2010a, b). Before this mass extinction, biodiversity increased in the Early Guadalupian (Roadian) and then declined gradually from the Middle Guadalupian (Wordinian) to the middle Capitanian (Late Guadalupian) (Groves and Wang 2013). Except for the anoxia (Zhang et al. 2015; Wei et al. 2016), large-scale volcanism such as the Emeishan large igneous province (LIP) had been suggested to be the main potential cause for this mass extinction (Wignall et al. 2009; Huang et al. 2018; Chen and Xu 2019). The volcanic greenhouse gases from the Emeishan LIP disturbed the global carbon cycle and caused a large carbon-isotope negative excursion from the mid-Capitanian to the G–L boundary (Wang et al. 2004; Bond et al. 2010b; Shen et al. 2013), though the global nature of this negative excursion had been questioned (Jost et al. 2014). Did this

✉ Hengye Wei
weihengye@163.com

¹ School of Geoscience and Technology, Southwest Petroleum University, Chengdu 610500, China

² School of Earth Science, East China University of Technology, Nanchang 330013, China

carbon-isotope negative excursion take place from a long-term carbon cycle stability or reflect carbon cycle perturbations which started from the Early and Middle Guadalupian? Addressing this question will assist in the understanding of the causes for this mass extinction, as the Early-Middle Guadalupian marine environmental conditions before the mass extinction event seems to be essential (Musashi et al. 2010). The ocean processes that interact with the global carbon cycle affect the chemical- and physical-conditions of bottom water where benthic faunas lived during the Guadalupian crisis.

The transfer of organic carbon in the ocean is forced by biological pump regulated by climate changes (Goodwin et al. 2008). During this process, organic carbon hiding in the sediments keeps oxygen in the atmosphere (Hemingway et al. 2019). Therefore, the stable isotopic composition of organic matter is often used for the reconstruction of paleoclimates and paleoceanography in the past (Arthur et al. 1988; Popp et al. 1997; Hayes et al. 1999; Dawson et al. 2002; Galimov 2006). The covariance of carbon-isotope composition from carbonate rocks and organic matter can be used to support for global carbon changes (Dean et al. 1986; Freeman and Hayes 1992; Magaritz et al. 1992; Holser 1997; Kump and Arthur 1999). Unfortunately, most of the carbon isotope studies in the Guadalupian had been inorganic-carbon isotope analyses (Wang et al. 2004; Isozaki et al. 2007; Bond et al. 2010b; Shen et al. 2013; Liu et al. 2017; Cao et al. 2018). A few studies of organic-carbon isotopic compositions had focused on the G–L boundary or the Capitanian (Kaiho et al. 2005; Bond et al. 2015), the Early Guadalupian (Liu et al. 2018), or the Early-Middle Guadalupian with low-resolution samples (Birgenheier et al. 2010; Zhang et al. 2020).

We present here organic-carbon isotope stratigraphy in the Guadalupian from two separated sections (Chaohu and Xiaolao) in the Lower Yangtze area, South China. We also analyzed TOC and H contents to constrain the organic-carbon isotopic variations. Our results will help to analyze the global carbon cycle during the Guadalupian, and to constrain the environmental changes during the Guadalupian biocrisis for a better understanding of mass extinction causes.

2 Geological setting

During the Guadalupian, the South China block was a large tropical isolated platform located in the east of the Paleo-Tethys Ocean (Fig. 1a). The South China block is composed of the carbonate Yangtze Platform in the west and the arenaceous Cathaysia Platform in the east. The Lower Yangtze area was located in the northeast part of the South

China block (Fig. 1b). This area was framed by the Jiangshao fault in the east and the Tanlu fault in the west (He et al. 2014). During the Middle Permian, the depression of this area formed the Lower Yangtze Basin, which deposited deep-water facies of the black cherts in the Kuhfeng Formation (Li et al. 2008).

The two studied sections at Chaohu ($25^{\circ} 01' 44''$ N, $113^{\circ} 44' 18''$ E) and Xiaolao ($30^{\circ} 56' 47''$ N, $118^{\circ} 0' 52''$ E) were located in the deep basin and the platform slope environments, respectively (Fig. 1b). At the Chaohu section, the Cisuralian Chihsia Formation, the Guadalupian Kuhfeng, and the Yingping formations outcrop in ascending order (Fig. 2), where the Kuhfeng Formation is the main studied interval. The upper Chihsia Formation consists of gray bioclastic limestones with abundant crinoids, foraminifers, fusulinids, ostracods, brachiopods, and some gastropods and bivalves. The contact between the Chihsia and the Kuhfeng is separated by an unconformity, suggesting a hiatus. At the base of the Kuhfeng Formation, brown mudstones intercalated with several layers of bentonites are of the age 272.95 ± 0.11 Ma and 271.038 ± 0.097 Ma (Wu et al. 2017), suggesting the base of the Guadalupian epoch (Shen et al. 2019). The lower Kuhfeng Formation consists of black muddy cherts with abundant phosphorite nodules. Kametaka et al. (2005) inferred that these phosphorite nodules formed in dysoxic environments with low terrestrial detritus supply. The middle and upper Kuhfeng Formation consists of thin-bedded black cherts with high organic matter content (Fig. 2). The Kuhfeng Formation contains abundant radiolarians and sponge spicules. Radiolarian assemblage studies suggest that the Kuhfeng Formation spans the Roadian to the middle Capitanian stages (He et al. 1999; Kametaka et al. 2009). At the top of the Kuhfeng Formation, several cm-scale bentonite layers have an age of 261.6 ± 1.5 Ma (Zhang et al. 2019). The contact between the Kuhfeng and Yingping formations is conformable. The Yingping Formation consists of dark-gray shales which turn into mixed colors of purple, dark-gray and white altered by modern weathering.

At the Xiaolao section, the Cisuralian Chihsia Formation and the Guadalupian Kuhfeng Formation outcrop in ascending order (Fig. 2). The upper Chihsia Formation consists of medium- to thick-bedded grey limestones with abundant foraminifers, bryozoans, ostracods, and green algae. The contact between the Chihsia and Kuhfeng formations is conformable. The lower Kuhfeng Formation consists of thin- to medium-bedded cherty limestones and black shales with phosphorite nodules which can be correlated with the phosphorite nodules interval in the lower Kuhfeng Formation at Chaohu section, ~ 85 km away. The middle Kuhfeng Formation consists of gray to dark-gray thin-bedded cherts with rare radiolarians and common sponge spicules. The upper Kuhfeng Formation consists of

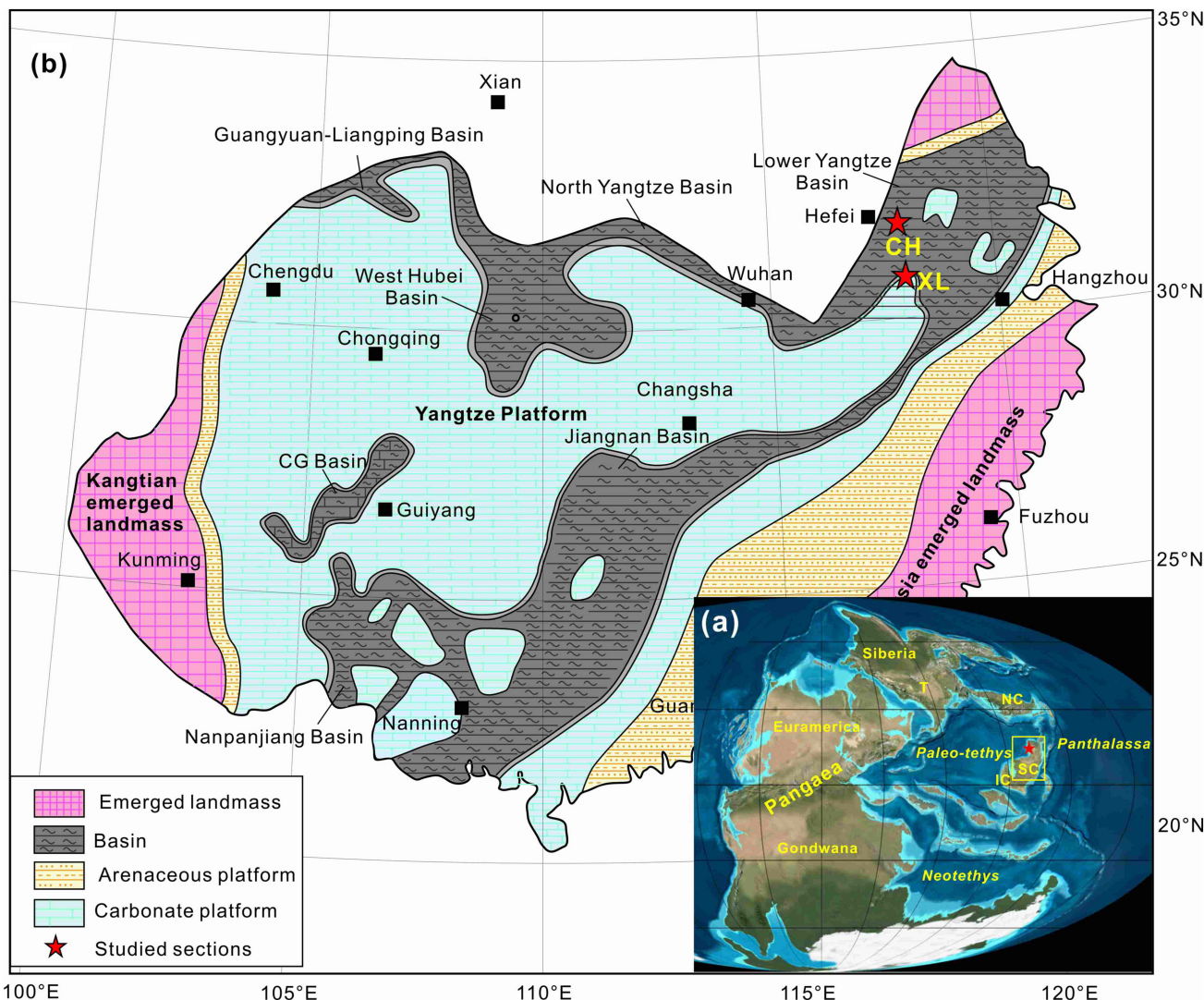


Fig. 1 **a** Guadalupian global paleogeography. SC South China. NC North China. IC Indochina. T Tarim. CG Central Guizhou. Base map courtesy of Ron Blakey (<http://jan.ucc.nau.edu/~rcb7/>). Note: 70° counterclockwise of South China block relative to its modern orientation (Nie 1991). **b** Guadalupian paleogeography of South China (modified from Wei et al. (2016) and Chen et al. (2018)). CH Chaohu, XL Xiaolao. The base map with coordinate was adapted from Google maps

gray medium-bedded nodular cherts containing sponge spicules and ostracods. According to the stratigraphic characteristics of the Lower Yangtze area (Li et al. 2008), the upper Kuhfeng Formation is the transition interval between the Kuhfeng and the Wuxue formations, the latter is upper Capitanian limestone deposition. Therefore, the Kuhfeng Formation at Xiaolao spans from the Roadian to the middle Capitanian.

3 Methods

We collected samples from the upper Chihsia to the whole Kuhfeng formations. The samples were cleaned, dried, and then ground in an agate ball mill. Powdered samples were

digested by 2 N HCl to remove carbonate and then treated with HF to remove chert at 50 °C for more than 48 h. The residues were washed using 18.2 MΩ water until pH was neutral, and then centrifuged and dried for measurements of total organic carbon (TOC) and H contents, and bulk organic-carbon isotope ratios. The residues sample splits were used to analyze TOC and H contents by a Vario ELIII elemental analyzer at the Key Laboratory of Tectonics and Petroleum Resources of Ministry of Education, China University of Geosciences, Wuhan. Absolute precision for TOC and H is better than 0.3 %. For organic-carbon isotopic composition measurement, the residues sample splits were combusted at 800 °C and the released CO₂ was used to determine ¹³C/¹²C ratios using a Thermo Scientific MAT 253 at the Nanjing Institute of Geology and Palaeontology,

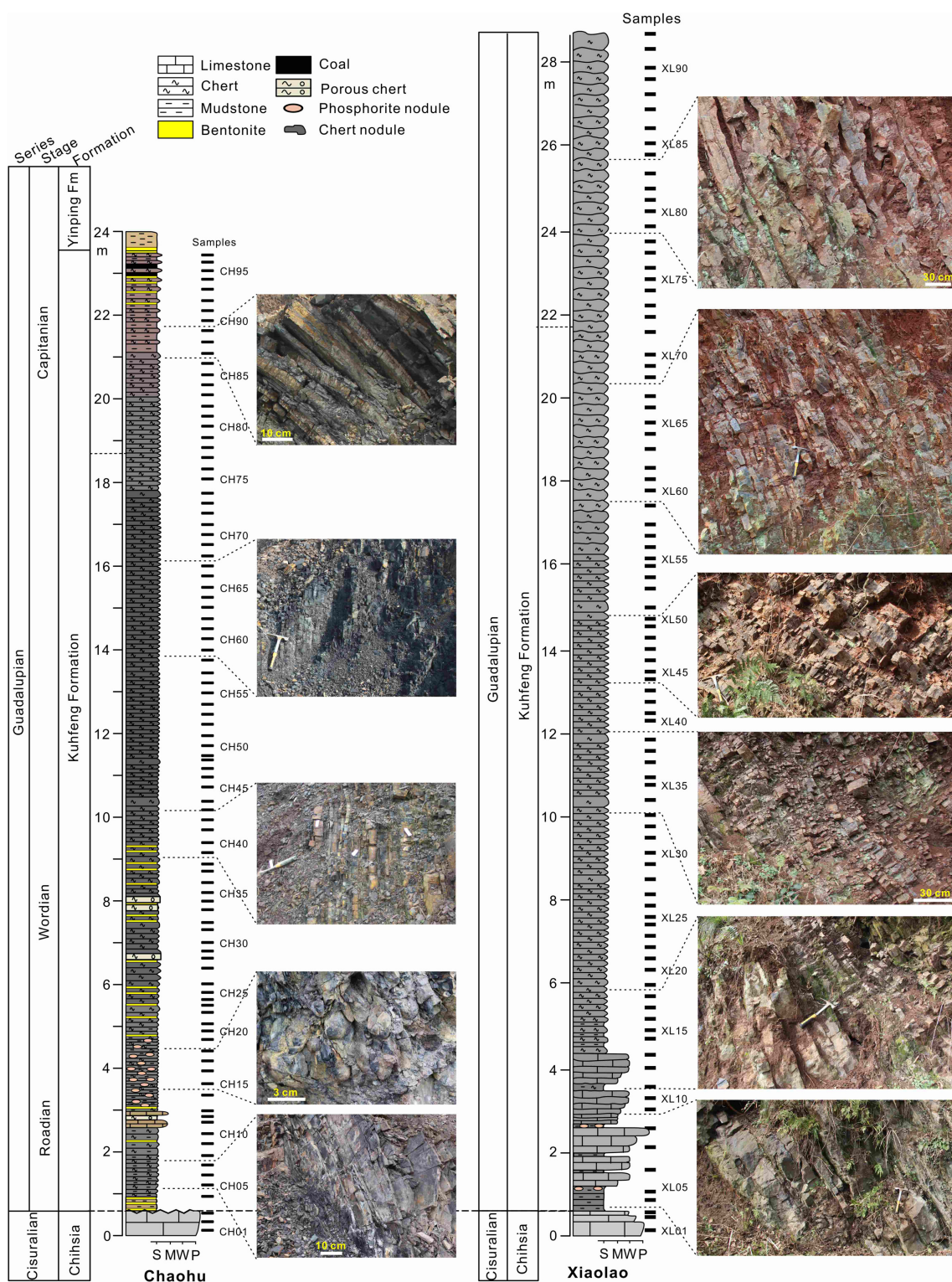


Fig. 2 Lithological logs and field photos at the Chaohu and Xiaolao sections, South China

Chinese Academy of Sciences. All the data are reported in per mille (‰) relative to the Vienna Pee Dee Belemnite (V-PDB) standard. The precision was better than $\pm 0.2\text{ ‰}$ based on the duplicate analyses of samples and standards of charcoal (GBW04407, -22.43 ‰) and urea (IVA3380217, -40.81 ‰).

4 Results

At the Chaohu section, TOC contents range from 0.03 % to 0.11 % in the Chihsia Formation and range from 0.48 % to 21.48 % (average = 4.52 %) in the Kuhfeng Formation (Table 1). The TOC profile shows two peaks in the lower and upper Kuhfeng Formation, respectively (Fig. 3). H contents range from 0.01 % to 0.05 % in the Chihsia Formation, and range from 0.15 % to 1.30 % (average = 0.37 %) in the Kuhfeng Formation. Atomic H/C ratios range from 1.21 to 5.66 in the Chihsia Formation and range from 0.26 to 5.56 (average = 1.87) in the Kuhfeng Formation. Bulk organic-carbon isotopic compositions ($\delta^{13}\text{C}_{\text{org}}$) range from -28.7 to -24.8 ‰ (average = -26.9 ‰). The $\delta^{13}\text{C}_{\text{org}}$ profile shows a peak in the lower Kuhfeng Formation and then a gradually decreasing trend upward (Fig. 3).

At Xiaolao section, TOC contents range from 0.15 % to 0.33 % in the Chihsia Formation, and range from 0.03 % to 0.66 % (average = 0.22 %) in the Kuhfeng Formation (Table 2). The TOC profile shows a weak decreasing trend upward (Fig. 3). H contents range from 0.01 % to 0.04 % in the Chihsia Formation, and range from 0.01 % to 0.62 % (average = 0.21 %) in the Kuhfeng Formation. Atomic H/C ratios range from 0.32 to 34.34 (average = 12.12). Bulk organic-carbon isotopic compositions ($\delta^{13}\text{C}_{\text{org}}$) range from -27.9 to -24.1 ‰ (average = -25.8 ‰). The $\delta^{13}\text{C}_{\text{org}}$ profile shows a peak in the lower Kuhfeng Formation and then a gradually decreasing trend upward, which is similar to the $\delta^{13}\text{C}_{\text{org}}$ profile trend at Chaohu (Fig. 3).

5 Discussion

5.1 Diagenetic effect on $\delta^{13}\text{C}_{\text{org}}$

Owing to selective preservation of organic matter through microbial decomposition during early diagenesis, sedimentary bulk organic matter $\delta^{13}\text{C}_{\text{org}}$ undergoes diagenetic alteration (Benner et al. 1987; Lehmann et al. 2002). However, there is a slight change (less than 1–2 ‰) of bulk organic-carbon isotopic composition during early diagenesis (Galimov 2006). Thermal alteration during late diagenesis tends to remove ^{13}C -depleted hydrocarbons and

increase the bulk organic carbon isotope compositions (Hayes et al. 1999; Tocqué et al. 2005). Biomarker studies on the organic matter in the Kuhfeng Formation in the Lower Yangtze area show a small change of thermal maturation (Geng and Wei 2019). This suggests that the significant $\delta^{13}\text{C}_{\text{org}}$ variations ($> 2.5\text{ ‰}$) here are likely unrelated to thermal alteration. Lehmann et al. (2002) concluded that bulk organic-carbon isotopic compositions are well correlated with primary isotope values, suggesting that sedimentary bulk organic-carbon isotope composition recorded surface waters signals. Furthermore, thermal alteration may only elevate absolute $\delta^{13}\text{C}_{\text{org}}$ values but not destroy secular trends (Des Marais et al. 1992). Therefore, the carbon composition of the organic matter here can be used to trace primary environmental changes (e.g., Ostrom et al. 1997; Hodell and Schelske 1998; Hayes 2004; Galimov 2006).

5.2 Global environmental controls on $\delta^{13}\text{C}_{\text{org}}$

In addition to diagenesis effect, several primary environmental factors could cause shifts in bulk organic-carbon isotopic composition, including the mixture of marine organic and terrestrial C₃ carbon, initial $\delta^{13}\text{C}$ of carbon source, photosynthetic fractionation and rate of organic matter burial (Arthur et al. 1985; Hayes et al. 1999; Newton and Bottrell 2007). First, in terms of organic matter provenance, terrestrial C₃ plant photosynthesis yields more (e.g. $\sim 10\text{ ‰}$) depleted $\delta^{13}\text{C}$ values of leaves than marine photosynthesis owing to the ^{13}C -depleted carbon source in the atmosphere relative to DIC and faster diffusion of CO₂ in the air relative to that in water (Newton and Bottrell 2007; Ohkouchi et al. 2015). Therefore, proportions of marine and terrestrial organic matter influence organic-carbon isotopic composition in sediments (Arthur et al. 1985; Hayes et al. 1999), and marine organic matter $\delta^{13}\text{C}$ is higher than terrestrial organic matter (Deines 1980). However, marine organic carbon that is Cretaceous or older is isotopically lighter than land-derived carbon (Dean et al. 1986; Galimov 2006; see also Cui et al. 2017). Permian higher plants show heavier $\delta^{13}\text{C}$ values than coeval marine-derived organic matter (Hayes et al. 1999; Krull 1999; Ward et al. 2005; Kraus et al. 2013). This opposite trend can be interpreted by (1) marine organic-carbon $\delta^{13}\text{C}$ values older than Cenozoic are more negative than marine organic carbon in most Cenozoic sediments because of higher atmospheric CO₂ concentrations and thus higher isotopic fractionation (Arthur et al. 1985; Popp 1989; Hayes et al. 1999); (2) the whole-plant $\delta^{13}\text{C}$ values in sedimentary organic matter are heavier than leaves (Badeck et al. 2005; Cernusak et al. 2009); (3) gymnosperms $\delta^{13}\text{C}$ values are more ^{13}C -enriched than angiosperms which bloom in Cenozoic (Diefendorf et al. 2010),

Table 1 TOC, atomic H/C ratio and organic-carbon isotopic composition data at Chaohu section, South China

Sample	Formation	TOC (%)	H (%)	H/C (atom)	$\delta^{13}\text{C}$ (‰)	Sample	Formation	TOC (%)	H (%)	H/C (atom)	$\delta^{13}\text{C}$ (‰)
CH01	Chihsia	0.10	0.01	1.21	– 28.7	CH50	Kuhfeng	2.77	0.19	0.84	– 27.1
CH02	Chihsia	0.03	0.01	4.23	– 28.3	CH51	Kuhfeng	2.48	0.30	1.48	– 26.7
CH03	Chihsia	0.11	0.05	5.66	– 27.3	CH52	Kuhfeng	1.93	0.44	2.71	– 26.8
CH04	Kuhfeng	8.43	0.93	1.33	– 26.0	CH53	Kuhfeng	2.71	0.34	1.52	– 27.4
CH05	Kuhfeng	6.23	0.53	1.02	– 25.9	CH54	Kuhfeng	4.40	0.28	0.75	– 27.2
CH06	Kuhfeng	6.69	0.51	0.92	– 25.6	CH55	Kuhfeng	3.41	0.22	0.78	
CH07	Kuhfeng	7.26	0.64	1.06	– 25.7	CH56	Kuhfeng	3.39	0.28	1.00	– 27.2
CH08	Kuhfeng	3.35	0.39	1.38	– 26.4	CH57	Kuhfeng	3.60	0.36	1.19	– 27.6
CH09	Kuhfeng	6.64	0.62	1.12	– 26.3	CH58	Kuhfeng	3.56	0.33	1.13	– 26.8
CH10	Kuhfeng	15.44	0.85	0.66	– 25.3	CH59	Kuhfeng	6.40	0.24	0.44	– 27.1
CH11	Kuhfeng	0.48	0.20	4.92	– 26.4	CH60	Kuhfeng	5.58	0.51	1.09	– 26.0
CH12	Kuhfeng	9.64	0.94	1.17	– 26.0	CH61	Kuhfeng	8.24	0.37	0.54	– 27.1
CH13	Kuhfeng	6.53	0.75	1.37		CH62	Kuhfeng	13.16	0.29	0.26	– 26.2
CH14	Kuhfeng	4.40	0.51	1.40	– 25.8	CH63	Kuhfeng	10.08	0.46	0.55	– 26.3
CH15	Kuhfeng	17.36	1.03	0.71	– 24.8	CH64	Kuhfeng	4.47	0.33	0.88	– 26.3
CH16	Kuhfeng	16.55	0.80	0.58		CH65	Kuhfeng	8.42	0.24	0.35	
CH17	Kuhfeng	7.95	0.29	0.44	– 26.0	CH66	Kuhfeng	5.35	0.31	0.70	– 26.7
CH18	Kuhfeng	9.28	0.64	0.82	– 25.1	CH67	Kuhfeng	5.77	0.51	1.07	– 27.2
CH19	Kuhfeng	21.48	1.30	0.73	– 25.8	CH68	Kuhfeng	14.19	0.42	0.35	– 26.0
CH20	Kuhfeng	4.87	0.40	0.97	– 26.8	CH69	Kuhfeng	14.25	0.34	0.28	
CH21	Kuhfeng	2.57	0.25	1.14	– 26.6	CH70	Kuhfeng	11.35	0.46	0.48	– 26.1
CH22	Kuhfeng	1.88	0.46	2.92		CH71	Kuhfeng	14.70	0.38	0.31	– 26.2
CH23	Kuhfeng	2.13	0.41	2.32	– 26.7	CH72	Kuhfeng	9.25	0.40	0.51	– 27.3
CH24	Kuhfeng	1.59	0.27	2.03	– 26.5	CH73	Kuhfeng	11.96	0.34	0.34	– 26.7
CH25	Kuhfeng	3.57	0.26	0.88	– 27.0	CH74	Kuhfeng	12.42	0.32	0.31	– 26.7
CH26	Kuhfeng	2.66	0.27	1.21	– 26.9	CH75	Kuhfeng	8.04	0.38	0.57	– 26.5
CH27	Kuhfeng	1.31	0.34	3.09	– 27.9	CH76	Kuhfeng	2.59	0.28	1.32	– 26.6
CH28	Kuhfeng	0.80	0.27	4.02	– 28.0	CH77	Kuhfeng	0.82	0.30	4.37	– 27.2
CH29	Kuhfeng	2.02	0.33	1.97	– 26.8	CH78	Kuhfeng	1.67	0.41	2.95	– 26.3
CH30	Kuhfeng	2.06	0.28	1.62		CH79	Kuhfeng	2.76	0.30	1.30	
CH31	Kuhfeng	1.79	0.31	2.05	– 26.8	CH80	Kuhfeng	1.95	0.26	1.58	– 26.6
CH32	Kuhfeng	2.04	0.23	1.36	– 26.4	CH81	Kuhfeng	1.22	0.31	3.09	– 27.4
CH33	Kuhfeng	0.80	0.37	5.65	– 27.6	CH82	Kuhfeng	0.89	0.40	5.41	– 27.1
CH34	Kuhfeng	0.67	0.27	4.82	– 27.4	CH83	Kuhfeng	0.96	0.18	2.23	– 27.4
CH35	Kuhfeng	0.84	0.24	3.36		CH84	Kuhfeng	1.72	0.21	1.45	– 26.5
CH36	Kuhfeng	0.97	0.27	3.33	– 27.8	CH85	Kuhfeng	0.96	0.15	1.86	– 27.3
CH37	Kuhfeng	0.65	0.21	3.89	– 28.4	CH86	Kuhfeng	1.28	0.19	1.78	
CH38	Kuhfeng	1.73	0.24	1.69	– 27.2	CH87	Kuhfeng	1.90	0.23	1.47	– 27.4
CH39	Kuhfeng	1.34	0.22	1.98	– 26.5	CH88	Kuhfeng	1.62	0.19	1.42	– 27.3
CH40	Kuhfeng	1.53	0.34	2.69	– 26.9	CH89	Kuhfeng	1.44	0.23	1.92	– 27.6
CH41	Kuhfeng	1.16	0.18	1.87	– 27.7	CH90	Kuhfeng	1.04	0.46	5.35	– 27.5
CH42	Kuhfeng	1.96	0.21	1.27	– 26.6	CH91	Kuhfeng	0.72	0.25	4.12	– 27.5
CH43	Kuhfeng	1.03	0.34	3.95	– 27.8	CH92	Kuhfeng	0.89	0.16	2.19	– 27.9
CH44	Kuhfeng	1.11	0.25	2.75	– 26.9	CH93	Kuhfeng	1.27	0.31	2.89	– 27.5
CH45	Kuhfeng	2.05	0.26	1.55	– 26.7	CH94	Kuhfeng				– 27.6
CH46	Kuhfeng	1.03	0.28	3.25		CH95	Kuhfeng	1.18	0.21	2.10	– 27.8
CH47	Kuhfeng	1.02	0.42	4.89	– 28.2	CH96	Kuhfeng	1.30	0.39	3.56	– 27.7
CH48	Kuhfeng	1.19	0.29	2.92	– 28.0	CH97	Kuhfeng	1.01	0.39	4.64	– 28.2

Table 1 continued

Sample	Formation	TOC (%)	H (%)	H/C (atom)	$\delta^{13}\text{C}$ (‰)	Sample	Formation	TOC (%)	H (%)	H/C (atom)	$\delta^{13}\text{C}$ (‰)
CH49	Kuhfeng	3.43	0.40	1.41	–27.2						

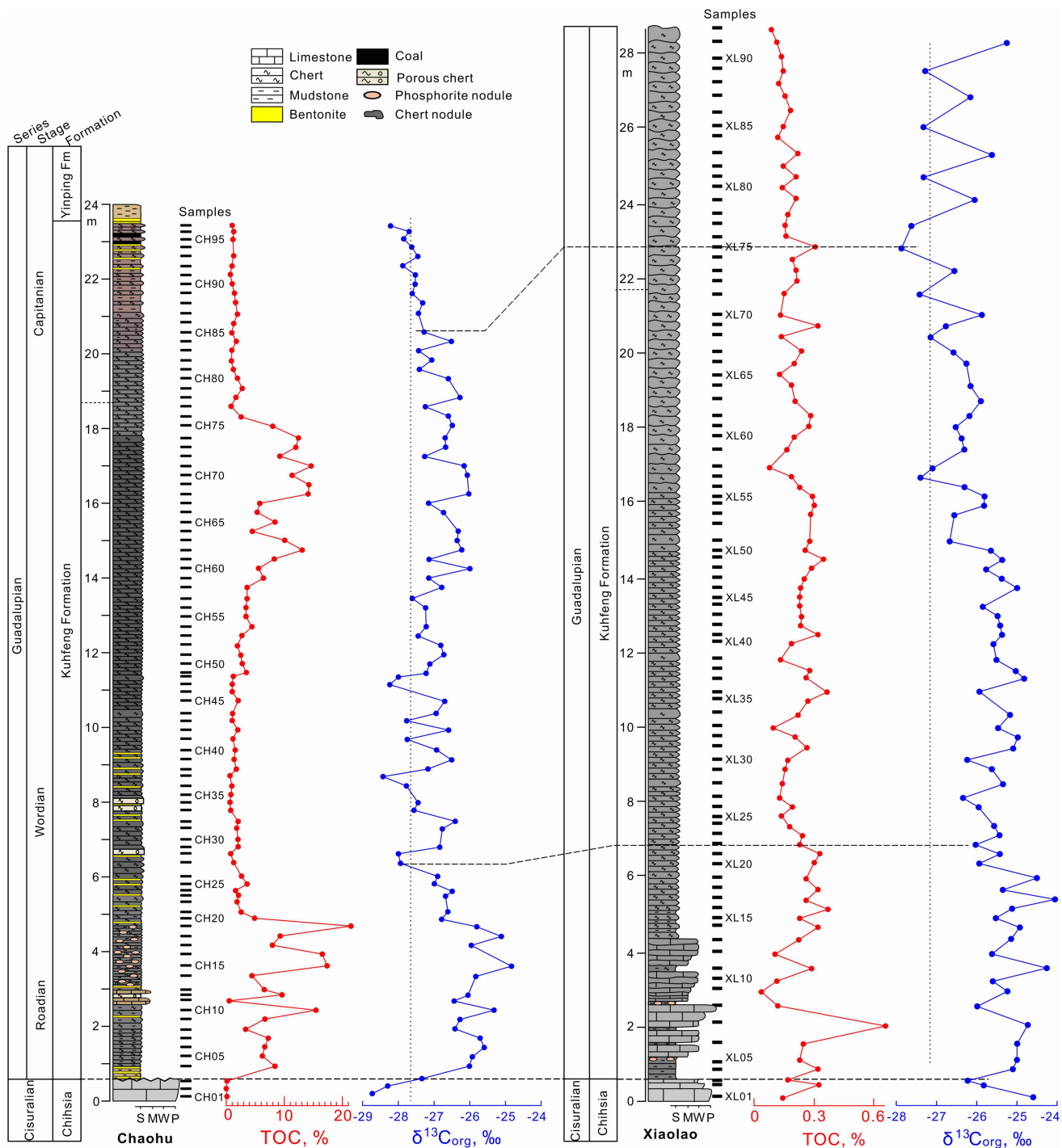
**Fig. 3** TOC and organic-carbon isotopic composition profiles at the Chaohu and Xiaolao sections, South China

Table 2 TOC, atomic H/C ratios and organic-carbon isotopic composition data at Xiaolao section, South China

Sample	Formation	TOC (%)	H (%)	H/C (atom)	$\delta^{13}\text{C}$ (‰)	Sample	Formation	TOC (%)	H (%)	H/C (atom)	$\delta^{13}\text{C}$ (‰)
XL01	Chihsia	0.15	0.02	1.92	– 24.6	XL47	Kuhfeng	0.25	0.15	7.05	– 25.4
XL02	Chihsia	0.33	0.01	0.32	– 25.8	XL48	Kuhfeng	0.29	0.25	10.55	– 25.8
XL03	Chihsia	0.17	0.04	2.51	– 26.2	XL49	Kuhfeng	0.35	0.15	5.04	– 25.4
XL04	Kuhfeng	0.32	0.19	7.25	– 25.1	XL50	Kuhfeng	0.26	0.41	19.21	– 25.6
XL05	Kuhfeng	0.23	0.22	11.54	– 25.0	XL51	Kuhfeng	0.28	0.37	15.79	– 26.7
XL06	Kuhfeng	0.25	0.04	1.91	– 25.0	XL53	Kuhfeng	0.28	0.23	– 26.6	
XL07	Kuhfeng	0.66	0.07	1.23	– 24.7	XL54	Kuhfeng	0.30	0.26	10.88	– 25.8
XL08	Kuhfeng	0.12	0.03	3.19	– 26.0	XL55	Kuhfeng	0.29	0.14	5.50	– 25.8
XL09	Kuhfeng	0.03	0.01	3.95	– 25.2	XL56	Kuhfeng	0.23	0.38	15.84	– 26.3
XL10	Kuhfeng	0.11	0.01	1.07	– 25.6	XL57	Kuhfeng	0.19	0.22	11.86	– 27.4
XL11	Kuhfeng	0.29	0.19	8.11	– 24.3	XL58	Kuhfeng	0.08	0.12	7.57	– 27.1
XL12	Kuhfeng	0.10	0.00	0.37	– 25.6	XL59	Kuhfeng	0.16	0.16	24.18	– 26.3
XL13	Kuhfeng	0.22	0.01	0.44	– 25.1	XL60	Kuhfeng	0.20	0.38	27.89	– 26.4
XL14	Kuhfeng	0.32	0.25	9.46	– 24.9	XL61	Kuhfeng	0.28	0.23	14.02	– 26.5
XL15	Kuhfeng	0.23	0.23	11.89	– 25.5	XL62	Kuhfeng	0.28	0.19	8.46	– 26.2
XL16	Kuhfeng	0.37	0.27	8.68	– 25.1	XL63	Kuhfeng	0.21	0.16	6.80	– 25.9
XL17	Kuhfeng	0.26	0.40	18.63	– 24.1	XL64	Kuhfeng	0.19	0.13	7.65	– 26.2
XL18	Kuhfeng	0.32	0.62	23.21	– 25.3	XL65	Kuhfeng	0.13	0.15	9.82	
XL19	Kuhfeng	0.26	0.15	6.96	– 24.5	XL66	Kuhfeng	0.20	0.09	8.49	– 26.3
XL20	Kuhfeng	0.30	0.24	9.44	– 25.9	XL67	Kuhfeng	0.24	0.16	9.60	– 26.6
XL21	Kuhfeng	0.33	0.33	12.09	– 25.4	XL68	Kuhfeng	0.14	0.18	9.34	– 27.1
XL22	Kuhfeng	0.23	0.19	9.78	– 26.0	XL69	Kuhfeng	0.32	0.30	25.87	– 26.8
XL23	Kuhfeng	0.24	0.26	12.87	– 25.4	XL70	Kuhfeng	0.13	0.28	10.39	– 25.9
XL24	Kuhfeng	0.18	0.22	14.77	– 25.6	XL71	Kuhfeng	0.15	0.35	31.57	– 27.4
XL25	Kuhfeng	0.14	0.14	12.63		XL72	Kuhfeng	0.22	0.14	11.01	
XL26	Kuhfeng	0.19	0.24	14.71	– 25.9	XL73	Kuhfeng	0.21	0.32	17.97	– 26.5
XL27	Kuhfeng	0.13	0.37	34.34	– 26.3	XL74	Kuhfeng	0.19	0.24	13.95	
XL28	Kuhfeng	0.14	0.15	12.45	– 25.3	XL75	Kuhfeng	0.30	0.29	17.87	– 27.9
XL29	Kuhfeng	0.16	0.14	10.40	– 25.6	XL76	Kuhfeng	0.16	0.14	5.48	
XL30	Kuhfeng	0.17	0.12	8.52	– 26.2	XL77	Kuhfeng	0.15	0.23	16.92	– 27.6
XL31	Kuhfeng	0.26	0.24	10.84	– 25.1	XL78	Kuhfeng	0.17	0.15	12.03	
XL32	Kuhfeng	0.21	0.13	7.81	– 25.0	XL79	Kuhfeng	0.21	0.15	10.91	– 26.0
XL33	Kuhfeng	0.10	0.18	22.70	– 25.5	XL80	Kuhfeng	0.14	0.43	24.24	
XL34	Kuhfeng	0.22	0.17	9.35	– 25.2	XL81	Kuhfeng	0.21	0.25	20.91	– 27.3
XL35	Kuhfeng	0.27	0.23	10.23		XL82	Kuhfeng	0.15	0.43	24.40	
XL36	Kuhfeng	0.37	0.16	5.29	– 25.9	XL83	Kuhfeng	0.22	0.20	16.29	– 25.6
XL37	Kuhfeng	0.26	0.13	5.85	– 24.8	XL84	Kuhfeng	0.12	0.28	15.24	
XL38	Kuhfeng	0.28	0.16	6.82	– 25.0	XL85	Kuhfeng	0.15	0.23	22.76	– 27.3
XL39	Kuhfeng	0.13	0.24	21.58	– 25.5	XL86	Kuhfeng	0.18	0.18	15.04	
XL40	Kuhfeng	0.19	0.27	16.93	– 25.6	XL87	Kuhfeng	0.15	0.20	13.30	– 26.2
XL41	Kuhfeng	0.32	0.26	9.59	– 25.4	XL88	Kuhfeng	0.12	0.20	15.31	
XL42	Kuhfeng	0.23	0.16	8.21	– 25.4	XL89	Kuhfeng	0.14	0.13	12.85	– 27.3
XL43	Kuhfeng	0.24	0.15	7.59	– 25.5	XL90	Kuhfeng	0.14	0.13	10.47	
XL44	Kuhfeng	0.23	0.13	6.65	– 25.8	XL91	Kuhfeng	0.11	0.19	16.65	– 25.2
XL45	Kuhfeng	0.23	0.13	6.90		XL92	Kuhfeng	0.09	0.23	24.35	
XL46	Kuhfeng	0.23	0.12	5.96	– 25.0				0.16	22.47	

and (4) vascular plants which bloom in Carboniferous and Permian are more $\delta^{13}\text{C}$ -enriched than non-vascular plants because of the $\delta^{13}\text{C}$ -enriched roots and woody stems (Cui et al. 2017).

In this study, we use atomic H/C ratios to indicate organic matter sources to constrain organic-carbon $\delta^{13}\text{C}$ variations. H/C ratios mainly reflect organic matter sources (Peters 1986; Talbot and Livingstone 1989) and thermal maturity (Baskin 1997). Marine autochthonous plankton organic matters consisting of proteins, carbohydrates, and lipids have high H/C ratios, while terrestrial higher plant organic matters consisting of lignin, cellulose, and scleroproteins have low H/C ratios (Stuermer et al. 1978; Deines 1980). The thermal maturity proxies of biomarkers of the Kuhfeng Formation in the Lower Yangtze area show a small variation upward (Geng and Wei 2019), and thus may not contribute to the significant variation of H/C ratios in this study. Cross-plots between organic matter $\delta^{13}\text{C}_{\text{org}}$ and H/C ratios show weak or no correlation in this study (Fig. 4), suggesting that organic matter sources exert a small impact on the $\delta^{13}\text{C}_{\text{org}}$ variations here. The terrestrial organic detrital grains in the Kuhfeng Formation are small and limited (Tang and Wei 2020), and the phosphorite nodules in the lower Kuhfeng Formation also suggest low terrestrial detritus input (Kametaka et al. 2005). Therefore, the gradually decreasing $\delta^{13}\text{C}_{\text{org}}$ trends upward in the Middle Permian Guadalupian here is unlikely to be due to changes of organic matter sources, but other factors.

Combining the $\delta^{13}\text{C}_{\text{org}}$ data at Chaohu and Xiaolao, the $\delta^{13}\text{C}_{\text{org}}$ trend of the Guadalupian in the Lower Yangtze area (South China) is matched by the inorganic-carbon $\delta^{13}\text{C}_{\text{carb}}$ trend in Guizhou (South China, Buggisch et al. 2011) (Fig. 5), suggesting that they are subject to the same forcing (Kump and Arthur 1999). Both of them show similar trends of a peak in the lower Roadian (see also

Zhang et al. 2020) and then a gradual negative shift of $\delta^{13}\text{C}$ upward (Fig. 5). Besides, inorganic-carbon isotopic composition from the Roadian to the Wordian in Japan (Musashi et al. 2010) and organic-carbon isotopic composition in the Guadalupian in Australia with low-resolution sampling (Birgenheier et al. 2010) also show a similar trend. Thus, the covariance of $\delta^{13}\text{C}$ measured on carbonate rocks and organic matter can argue for $\delta^{13}\text{C}$ changes during the global carbon cycle (Arthur et al. 1985; Magaritz et al. 1992; Holser 1997).

The global carbon isotopic composition changes in the Guadalupian are mainly affected by initial $\delta^{13}\text{C}$ values of DIC, marine photosynthetic fractionation and rate of organic burial (e.g., Arthur et al. 1985; Arens et al. 2000). Marine photosynthetic fractionation is related to DIC concentration (Dean et al. 1986) and organic matter amount during the biological pump process (Newton and Bottrell 2007). The Roadian cooling (Saunders and Reichow 2009; Chen et al. 2013) enhanced the oceanic upwelling intensity (Zhang et al. 2019), increasing the primary productivity and thus a peak in both inorganic- and organic-carbon isotopic compositions during this time (Fig. 5). Increasing $p\text{CO}_2$ and gradual global warming occurred from the late Roadian to the end-Guadalupian (Saunders and Reichow 2009; Chen et al. 2013), which resulted from basalt eruption in the opening of the Neo-Tethys Ocean (Muttoni et al. 2009), widespread subduction-related volcanism (Saunders and Reichow 2009), and the Emeishan large igneous province (LIP) eruption (Ali et al. 2005). Associated with the assembly of supercontinent Pangaea, the decreasing mountain belts (and the resultant reducing CO_2 consumption during silicate rocks weathering) also contribute to the increasing CO_2 in the Middle Permian (Saunders and Reichow 2009). The volcanic-release ^{12}C -enriched CO_2 would lower initial $\delta^{13}\text{C}$ of

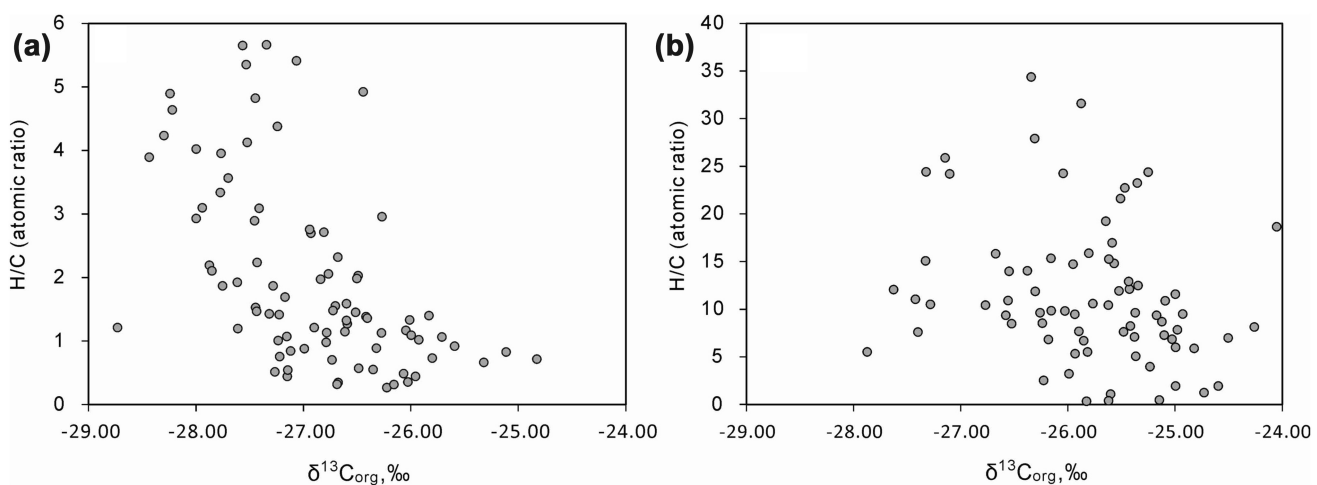


Fig. 4 Cross-plots between organic carbon isotope compositions and H/C ratios at the Chaohu (a) and Xiaolao (b) sections in South China

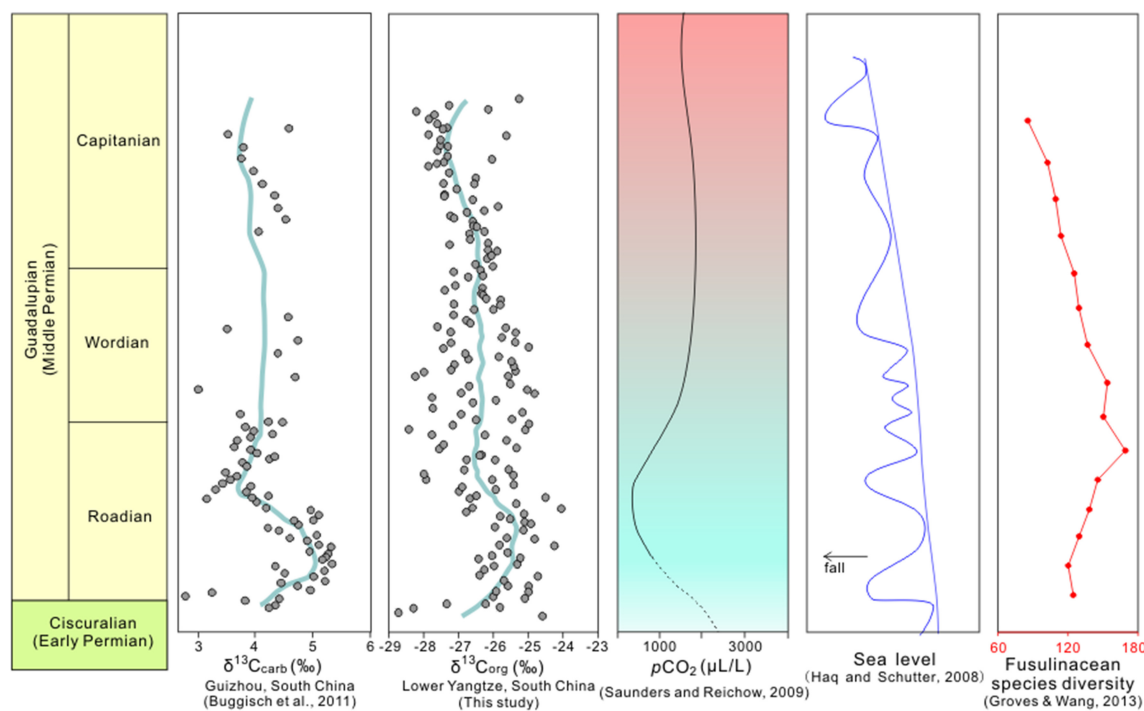


Fig. 5 $\delta^{13}\text{C}_{\text{org}}$ and $\delta^{13}\text{C}_{\text{carb}}$ correlation between the Lower Yangtze area (South China) and Guizhou (South China), and the atmospheric CO_2 concentration (Saunders and Reichow 2009), sea-level changes (Haq and Schutter 2008) and fusulinacean species diversity (Groves and Wang 2013) in the Guadalupian. The timescale and carbonate-carbon isotope of Guizhou are from Shen et al. (2019) and Buggisch et al. (2011). Organic-carbon isotope composition curves in this study are smoothed using LOESS smoothing procedure

marine DIC and contribute to the decreasing trend of $\delta^{13}\text{C}$ from the Roadian to the Capitanian (Fig. 5). Increasing $p\text{CO}_2$ in the Guadalupian atmosphere could increase marine DIC concentration (e.g., Brewer 1997; Wu et al. 2008). Greater CO_2 availability can enhance the extent of carbon-isotope fractionation by marine plankton (Dean et al. 1986), and thus produces more negative $\delta^{13}\text{C}$ values of organic matter. This may contribute to the observed negative shift of organic-carbon isotopic composition from the late Roadian to the Capitanian in the Guadalupian (Fig. 5). However, both the increased CO_2 concentration and the lower initial $\delta^{13}\text{C}$ value of DIC which resulted from volcanic-release CO_2 can only account for minor changes of 1–2 ‰ in the $\delta^{13}\text{C}$ of marine organic matter (Dean et al. 1986). The > 2.5 ‰ negative shift of $\delta^{13}\text{C}_{\text{org}}$ in the Guadalupian (Fig. 5) can be mainly controlled by other factor(s).

During the zenith process of the supercontinent Pangaea assembly in the Guadalupian (Isozaki 2009), global sea-level drop (Haq and Schutter 2008) caused drainage of coastal swamplands and reduced organic matter burial (Berner 2005; Peters-Kottig et al. 2006), resulting in more ^{12}C enrichment in DIC and thus a decrease of $\delta^{13}\text{C}_{\text{DIC}}$ and $\delta^{13}\text{C}_{\text{org}}$ via photosynthesis in the Guadalupian as seen in this study (e.g., Birgenheier et al. 2010; Buggisch et al. 2011, 2015). Meanwhile, the decomposition and oxidation

of organic matter to CO_2 during the sea-level drop could also contribute to the long-term $\delta^{13}\text{C}$ negative shift in the Guadalupian (e.g., Berner 2002), although some reports (Shields and Mills 2017; Zhang et al. 2020) suggest that a reduction of carbonate production during regression may drive a positive $\delta^{13}\text{C}$ excursion. The latter may offer a smaller contribution because dissolved inorganic carbon is smaller than dissolved organic carbon in rivers (Prokushkin et al. 2011). Dissolved organic matter (DOM) can form aggregates such as zooplankton shells and fecal pellets through faunas uptake (e.g., Alldredge and Silver 1988; Passow and Carlson 2012) to be fast-sinking particles (see review in Wakeham and Lee, 2019). The carbon-isotopic compositions of DOM are depleted in ^{13}C (Galimov 2006). Therefore, the sinking and burial efficiency of DOM can influence the carbon-isotopic compositions of marine carbonate and organic matter (D'Hondt et al. 1998). During the Guadalupian, the gradual decreasing diversity of benthic faunas led to decreased uptakes of DOM and thus may also contribute to the small $\delta^{13}\text{C}$ negative shift in the Capitanian in the Guadalupian (Fig. 5).

5.3 Implications for the Guadalupian mass extinction

The gradual negative shift of $\delta^{13}\text{C}$ in the Guadalupian (Fig. 5) and rapid $\delta^{13}\text{C}$ negative excursion at the end-Guadalupian (Wignall et al. 2009; Bond et al. 2010b; Shen et al. 2013) coincide with gradual extinction (Fig. 5, Groves and Wang 2013) and rapid extinction (Bond et al. 2010a; Shen and Shi 2009), respectively. This suggests a causal relationship. As mentioned above, the gradual negative shift of $\delta^{13}\text{C}$ from the Roadian to the middle Capitanian is mainly caused by decreased organic matter burial on land and in the ocean, which result from the global sea-level drop and oxygen-depletion-caused benthos decrease, respectively. The secondary causes for the gradual $\delta^{13}\text{C}$ negative shift are volcanic-gases release and decreased mountain belts, and thus decreased silicate weathering-consumption of CO_2 during this period (Chen and Xu 2019). Therefore, the gradual glacio-eustatic sea-level drop (Haq and Schutter 2008; Qiu et al. 2014) and reducing conditions of marine water masses (Wei et al. 2016, 2019) may be the causes for the gradual diversity-decreasing process in the Early and Middle Guadalupian. The significant $\delta^{13}\text{C}$ negative shift from the middle-late Capitanian to the end-Guadalupian inherits from the gradual negative shift in the Early and Middle Guadalupian, probably sharing the same causes for $\delta^{13}\text{C}$ variations of the Early-Middle Guadalupian. In other words, the significant $\delta^{13}\text{C}$ negative shift in the Late Guadalupian may be caused by the rapid global sea-level drop (Haq and Schutter 2008) and anoxia events (Zhang et al. 2015; Wei et al. 2016, 2019), which may be also the main causes for the rapid mass extinction during this time. Oxygen depletion can trigger sublethal to lethal effects (Riedel et al. 2008) and global sea-level drop caused geographic habitat loss (Haq and Schutter 2008). The combined effect of these two events likely led to the mass extinction.

6 Conclusions

We reconstructed marine organic-carbon isotopic composition changes in the Guadalupian through the study of two sections (Chaohu and Xiaolao) in the Lower Yangtze area, South China. Our results show that the $\delta^{13}\text{C}_{\text{org}}$ changes in the Guadalupian can be matched by $\delta^{13}\text{C}$ changes of carbonate rocks or organic matter in South China and other places in the world. Both inorganic- and organic-carbon isotopic compositions have similar trends in the Guadalupian, showing a peak in the Roadian and a gradual negative shift from the late Roadian to the middle Capitanian. The positive peak in the Roadian was probably due to high productivity caused by intensive upwelling from cooling

during this time. The gradual negative shift of $\delta^{13}\text{C}$ was mainly caused by decreased organic matter burial on land and in the ocean, which result from the global sea-level drop and anoxia-caused benthos decreasing, respectively. The secondary causes for the gradual $\delta^{13}\text{C}$ negative shift are volcanic-gases releasing, decreased mountain belts and thus decreased silicate weathering-consumption of CO_2 . The gradual negative shift of $\delta^{13}\text{C}$ coincides with the gradual extinction in the Guadalupian. Therefore, global sea-level drop and marine reducing conditions may be the main causes of the gradual diversity decrease in the Early and Middle Guadalupian.

Acknowledgements We thank two anonymous reviewers for their constructive comments. This work was funded by the National Natural Science Foundation of China (No. 41762003).

Compliance with ethical standards

Conflict of interest The authors declare that there is no conflict of interest regarding the publication of this paper.

References

- Ali JR, Thompson GM, Zhou MF, Song X (2005) Emeishan large igneous province, SW China. *Lithos* 79:475–489
- Allredge AL, Silver MW (1988) Characteristics, dynamics and significance of marine snow. *Prog Oceanogr* 20:41–82
- Arens NC, Jahren AH, Amundson R (2000) Can C3 plants faithfully record the carbon isotopic composition of atmospheric carbon dioxide? *Paleobiology* 26:137–164
- Arthur MA, Dean WE, Claypool GE (1985) Anomalous ^{13}C enrichment in modern marine organic carbon. *Nature* 295:216–218
- Arthur MA, Dean WE, Pratt LM (1988) Geochemical and climatic effects of increased marine organic carbon burial at the Cenomanian/Turonian boundary. *Nature* 335:714–717
- Badeck FW, Tcherkez G, Nogues S, Piel C, Ghashghaie J (2005) Post-photosynthetic fractionation of stable carbon isotopes between plant organs—a widespread phenomenon. *Rapid Commun Mass Spectrom* 19:1381–1391
- Baskin DK (1997) Atomic H/C ratio of kerogen as an estimate of thermal maturity and organic matter conversion. *AAPG Bull* 81:1437–1450
- Benner R, Fogel ML, Sprague EK, Hodson RE (1987) Depletion of ^{13}C in lignin and its implications for stable isotope studies. *Nature* 329:708–710
- Berner RA (2002) Examination of hypotheses for the Permo-Triassic boundary extinction by carbon cycle modeling. *Proc Natl Acad Sci USA* 99:4172–4177
- Berner RA (2005) The carbon and sulfur cycles and atmospheric oxygen from middle Permian to middle Triassic. *Geochim Cosmochim Acta* 69:3211–3217
- Birgenheier LP, Frank TD, Fielding CR, Rygel MC (2010) Coupled carbon isotopic and sedimentological records from the Permian system of eastern Australia reveal the response of atmospheric carbon dioxide to glacial growth and decay during the late Paleozoic Ice Age. *Palaeogeogr Palaeoclimatol Palaeoecol* 286:178–193

- Bond PGD, Hilton J, Wignall PB, Ali JR, Stevens LG, Sun Y, Lai X (2010a) The Middle Permian (Capitanian) mass extinction on land and in the oceans. *Earth Sci Rev* 102:100–116
- Bond DPG, Wignall PB, Wang W, Izon G, Jiang H, Lai X, Sun Y, Newton RJ, Shao L, Védrine S, Cope H (2010b) The mid-Capitanian (Middle Permian) mass extinction and carbon isotope record of South China. *Palaeogeogr Palaeoclimatol Palaeoecol* 292:282–294
- Bond DPG, Wignall PB, Joachimski MM, Sun Y, Savov I, Grasby SE, Beauchamp B, Blomeier DPG (2015) An abrupt extinction in the Middle Permian (Capitanian) of the Boreal Realm (Spitsbergen) and its link to anoxia and acidification. *Geol Soc Am Bull* 127:1411–1421
- Brewer PG (1997) Ocean chemistry of the fossil fuel CO₂ signal: the haline of “business as usual”. *Geophys Res Lett* 24:1367–1369
- Buggisch W, Wang X, Alekseev AS, Joachimski MM (2011) Carboniferous-Permian carbon isotope stratigraphy of successions from China (Yangtze platform), USA (Kansas) and Russia (Moscow Basin and Urals). *Palaeogeogr Palaeoclimatol Palaeoecol* 301:18–38
- Buggisch W, Krainer K, Schaffhauser M, Joachimski M, Korte C (2015) Late Carboniferous to Late Permian carbon isotope stratigraphy: a new record from post-Variscan carbonates from the Southern Alps (Austria and Italy). *Palaeogeogr Palaeoclimatol Palaeoecol* 433:174–190
- Cao C, Cui C, Chen J, Summons RE, Shen S, Zhang H (2018) A positive C-isotope excursion induced by sea-level fall in the middle Capitanian of South China. *Palaeogeogr Palaeoclimatol Palaeoecol* 505:305–316
- Cernusak LA, Tcherkez G, Keitel C, Comwell WK, Santiago LS, Knoblauch A, Barbour MM, Williams DG, Reich PB, Ellsworth DS (2009) Why are non-photosynthetic tissues generally ¹³C enriched compared with leaves in C₃ plants? Review and synthesis of current hypotheses. *Funct Plant Biol* 36:199–213
- Chen J, Xu Y (2019) Establishing the link between Permian volcanism and biodiversity changes: insights from geochemical proxies. *Gondwana Res* 75:68–95
- Chen B, Joachimski MM, Shen S, Lambert LL, Lai X, Wang X, Chen J, Yuan D (2013) Permian ice volume and palaeoclimate history: oxygen isotope proxies revisited. *Gondwana Res* 44(1):77–89
- Chen F, Xue W, Yan J, Wignall PB, Meng Q, Luo J, Feng Q (2018) Alatoconchids: giant Permian bivalves from South China. *Earth Sci Rev* 179:147–167
- Clapham ME (2015) Ecological consequences of the Guadalupian extinction and its role in the brachiopod-mollusk transition. *Paleobiology* 41:266–279
- Cui Y, Bercovici A, Yu J, Kump LR, Freeman KH (2017) Carbon cycle perturbation expressed in terrestrial Permian-Triassic boundary sections in South China. *Glob Planet Change* 148:272–285
- D'Hondt S, Donaghay P, Zachos JC, Luttenberg D, Lindinger M (1998) Organic carbon fluxes and ecological recovery from the Cretaceous-Tertiary mass extinction. *Science* 282:276–279
- Dawson TE, Mambelli S, Plamboeck AU, Templer PU, Tu KP (2002) Stable isotopes in plant ecology. *Ann Rev Ecol Syst* 33:507–559
- Dean ED, Arthur MA, Claypool GE (1986) Depletion of ¹³C in Cretaceous marine organic matter: source, diagenetic, or environmental signal? *Mar Geol* 7:119–157
- Deines P (1980) The isotopic composition of reduced organic carbon. In: Fritz P, Fontes J (eds) *Handbook of environmental isotope geochemistry*, vol 1. Elsevier, Amsterdam, pp 329–406
- Des Marais DJ, Strauss H, Humons RE, Hayes J (1992) Carbon isotope evidence for the stepwise oxidation of the Proterozoic environment. *Nature* 359:605–609
- Diefendorf AF, Mueller KE, Wing SL, Freeman KH (2010) Global patterns in leaf ¹³C discrimination and implications for studies of past and future climate. *Proc Natl Acad Sci USA* 107:5738–5743
- Freeman KH, Hayes JM (1992) Fractionation of carbon isotopes by phytoplankton and estimates of ancient pCO₂ levels. *Glob Biogeochem Cycles* 6:629–644
- Galimov EM (2006) Isotope organic geochemistry. *Org Geochem* 37:1200–1262
- Geng Z, Wei H (2019) Organic geochemical characteristics of organic-rich chert in the middle Permian Gufeng Formation in Chaohu, Lower Yangtze area. *Geol J China Univ* 25:823–837 (in Chinese)
- Goodwin P, Follows MJ, Williams RG (2008) Analytical relationships between atmospheric carbon dioxide, carbon emissions, and ocean processes. *Glob Biogeochem Cycles* 22(3):GB3030. <https://doi.org/10.1029/2008gb003184>
- Groves JR, Wang Y (2013) Timing and size selectivity of the Guadalupian (Middle Permian) fusulinoidean extinction. *J Paleontology* 87:183–196
- Haq BU, Schutter SR (2008) A chronology of Paleozoic sea-level changes. *Science* 322:64–68
- Hayes JM (2004) Isotopic order, biogeochemical processes, and earth history. *Geochim Cosmochim Acta* 68:1691–1700
- Hayes JM, Strauss H, Kaufman AJ (1999) The abundant of ¹³C in marine organic matter and isotopic fractionation in the global biogeochemical cycle of carbon during the past 800 Ma. *Chem Geol* 161:103–125
- He W, Wu S, Zhang K, Bu J (1999) Classification of radiolarian fossil zones and environmental analysis of Gufeng Formation in Lower Yangtze region. *Jiangsu Geol* 23:17–23 (in Chinese)
- He W, Tang T, Yue M, Deng J, Pan G, Xing G, Luo M, Xu Y, Wei Y, Zhang Z, Xiao Y, Zhang K (2014) Sedimentary and tectonic evolution of Nanhuan-Permian in South China. *J Earth Sci* 39:929–953 (in Chinese)
- Hemingway JD, Rothman DH, Grant KE, Rosengard SZ, Eglinton TI, Derry LA, Galley VV (2019) Mineral protection regulates long-term global preservation of natural organic carbon. *Nature* 570:228–231
- Hodell DA, Schelske CL (1998) Production, sedimentation, and isotopic composition of organic matter in Lake Ontario. *Limnol Oceanogr* 43:200–214
- Holser TW (1997) Geochemical events documented in inorganic carbon isotopes. *Palaeogeogr Palaeoclimatol Palaeoecol* 132:173–182
- Huang Y, Chen Z, Wignall PB, Grasby SE, Zhao L, Wang X, Kaiho K (2018) Biotic responses to volatile volcanism and environmental stresses over the Guadalupian–Lopingian (Permian) transition. *Geology* 47:175–178
- Isozaki Y (2009) Illawarra Reversal: the fingerprint of a superplume that triggered Pangean breakup and the end-Guadalupian (Permian) mass extinction. *Gondwana Res* 15:421–432
- Isozaki Y, Kawahata H, Ota A (2007) A unique carbon isotope record across the Guadalupian–Lopingian (Middle–Upper Permian) boundary in mid-oceanic paleo-atoll carbonates: the high-productivity “Kamura event” and its collapse in Panthalassa. *Global Planet Change* 55:21–38
- Jin Y, Zhang J, Shang Q (1994) Two phases of the end-Permian mass extinction. *Can Soc Pet Geol* 17:813–822
- Jost AB, Mundil R, He B, Brown ST, Altiner D, Sun Y, DePaolo DJ, Payne JL (2014) Constraining the cause of the end-Guadalupian extinction with coupled records of carbon and calcium isotopes. *Earth Planet Sci Lett* 396:201–212
- Kaiho K, Chen ZQ, Ohashi T, Arinobu T, Sawada K, Cramer BS (2005) A negative carbon isotope anomaly associated with the earliest Lopingian (Late Permian) mass extinction. *Palaeogeogr Palaeoclimatol Palaeoecol* 223:172–180

- Kametaka M, Takebe M, Nagai H, Zhu S, Takayanagi Y (2005) Sedimentary environments of the Middle Permian phosphorite-chert complex from the northeastern Yangtze plalform, China; the Gufeng Formation: a continental shelf radiolarian chert. *Sed Geol* 174:197–222
- Kametaka M, Nagai H, Zhu S, Takebe M (2009) Middle Permian radiolarians from the Anmenkou, Chaohu, Northeastern Yangtze platform, China. *Island Arc* 18:108–125
- Kraus SH, Brandner R, Heubeck C, Kozur HW, Struck U, Korte C (2013) Carbon isotope signatures of latest Permian marine successions of the Southern Alps suggest a continental runoff pulse enriched in land plant material. *Foss Rec* 16:97–109
- Krull ES (1999) Permian palsa mires as paleoenvironmental proxies. *Palaios* 14:530–544
- Kump L, Arthur MA (1999) Interpreting carbon-isotope excursions: carbonates and organic matter. *Chem Geol* 161:181–198
- Lehmann MF, Bernasconi SM, Barbieri A, McKenzie JA (2002) Preservation of organic matter and alteration of its carbon and nitrogen isotope composition during simulated and in situ early sedimentary diagenesis. *Geochim Cosmochim Acta* 66:3573–3584
- Li S, Meng Q, Wang Q, Kong W, He G (2008) Deposition of carbonate slope and ore-forming in Permian strata in the Middle-Lower Reaches of the Yangtze River, east China. *Acta Petrolo Sin* 24:1733–1744
- Liu C, Jarochowska E, Du Y, Vachard D, Munnecke A (2017) Stratigraphical and $\delta^{13}\text{C}$ records of Permo-Carboniferous platform carbonates, South China: responses to late Paleozoic icehouse climate and icehouse-greenhouse transition. *Palaeogeogr Palaeoclimatol Palaeoecol* 474:113–129
- Liu C, Du Y, Jarochowska E, Yan J, Munnecke A, Lu G (2018) A major anomaly in the carbon cycle during the late Cisuralian (Permian): timing, underlying triggers and implications. *Palaeogeogr Palaeoclimatol Palaeoecol* 491:112–122
- Magaritz M, Krishnamurthy RV, Holser WT (1992) Parallel trends in organic and inorganic carbon isotopes across the Permian/Triassic boundary. *Am J Sci* 292:727–739
- Musashi M, Isozaki Y, Kawahata H (2010) An Early-Middle Guadalupian (Permian) isotopic record from a mid-oceanic carbonate buildup: Akiyoshi Limestone, Japan. *Glob Planet Change* 73:114–122
- Muttoni G, Gaetani M, Kent DV, Sciunnach D, Angiolini L, Berra F, Garzani E, Mattei M, Zanchi A (2009) Opening of the Neo-Tethys Ocean and the Pangea B to Pangea A transformation during the Permian. *GeoArabia* 14:17–48
- Newton R, Bottrell S (2007) Stable isotopes of carbon and Sulphur as indicators of environmental change: past and present. *J Geol Soc Lond* 164:691–708
- Nie S (1991) Paleoclimatic and paleomagnetic constraints on the Paleozoic reconstructions of South China, North China and Tarim. *Tectonophysics* 196:279–308
- Ohkouchi N, Ogawa NO, Chikaraishi Y, Tanaka H, Wada E (2015) Biochemical and physiological bases for the use of carbon and nitrogen isotopes in environmental and ecological studies. *Prog Earth Planet Sci* 2:1
- Ostrom NE, Macko SA, Deibel D, Thompson RJ (1997) Seasonal variation in the stable carbon and nitrogen isotope biogeochemistry of a coastal cold ocean environment. *Geochim Cosmochim Acta* 61:2929–2942
- Passow U, Carlson CA (2012) The biological pump in a high CO_2 world. *Mar Ecol Prog Ser* 470:249–271
- Peters K (1986) Guidelines for evaluating petroleum source rock using programmed pyrolysis. *AAPG Bull* 70:318–329
- Peters-Kottig W, Strauss H, Kerp H (2006) The land plant $\delta^{13}\text{C}$ record and plant evolution in the Late Palaeozoic. *Palaeogeogr Palaeoclimatol Palaeoecol* 240:237–252
- Popp BN (1989) The post-Paleozoic chronology and mechanism of ^{13}C depletion in primary marine organic matter. *Am J Sci* 289:436–454
- Popp BN, Parekh P, Tilbrook B, Bidagare RR, Laws EA (1997) Organic carbon $\delta^{13}\text{C}$ variations in sedimentary rocks as chemostratigraphic and paleoenvironmental tools. *Palaeogeogr Palaeoclimatol Palaeoecol* 132:119–132
- Prokushkin AS, Pokrovsky OS, Shirokova LS, Korets MA, Viers J, Prokushkin SG, Amon RMW, Guggenberger G, McDowell WH (2011) Sources and the flux pattern of dissolved carbon in rivers of the Yenisey basin draining the Central Siberian Plateau. *Environ Res Lett* 6:045212
- Qiu Z, Wang Q, Zou C, Yan D, Wei H (2014) Transgressive-regressive sequences on the slope of an isolated carbonate platform (Middle-Late Permian, Laibin, South China). *Facies* 60:327–345
- Riedel B, Zuschin M, Haselmair A, Stachowitzsch M (2008) Oxygen depletion under glass: behavioural responses of benthic macrofauna to induced anoxia in the Northern Adriatic. *J Exp Mar Biol Ecol* 367:17–27
- Saunders A, Reichow M (2009) The Siberian Traps and the End-Permian mass extinction: a critical review. *Chin Sci Bull* 54:20–37
- Shen SZ, Shi GR (1996) Diversity and extinction patterns of of South China. *Hist Biol* 12:93–110
- Shen SZ, Shi GR (2002) Paleobiogeographical extinction patterns of Permian brachiopods in the Asian-western Pacific region. *Paleobiology* 28:449–463
- Shen SZ, Shi GR (2009) Latest Guadalupian brachiopods from the Guadalupian/Lopingian boundary GSSP section at Penglaitan in Laibin, Guangxi, South China and implications for the timing of the pre-Lopingian crisis. *Palaeoworld* 18:152–161
- Shen SZ, Cao C, Zhang H, Bowring SA, Henderson CM, Payne JL, Davydov VI, Chen B, Yuan D, Zhang Y, Wang W, Zheng Q (2013) High-resolution $\delta^{13}\text{C}_{\text{carb}}$ chemostratigraphy from latest Guadalupian through earliest Triassic in South China and Iran. *Earth Planet Sci Lett* 375:156–165
- Shen SZ, Zhang H, Zhang Y, Yuan D, Chen B, He W, Mu L, Lin W, Wang W, Chen J, Wu Q, Cao C, Wang Y, Wang X (2019) Permian integrative stratigraphy and timescale of China. *Scince China Earth Sci* 62:154–188
- Shields GA, Mills BJ (2017) Tectonic controls on the long-term carbon isotope mass balance. *Proc Natl Acad Sci USA* 144:4318–4323
- Stuermer DH, Peters KE, Kaplan IR (1978) Source indicator of humic substances and proto-kerogen. Stable isotope ratios, elemental compositions and electron spin resonance spectra. *Geochim Cosmochim Acta* 42:989–997
- Talbot MR, Livingstone DA (1989) Hydrogen index and carbon isotopes of lacustrine organic matter as lake level indicators. *Palaeogeogr Palaeoclimatol Palaeoecol* 70:121–137
- Tang Z, Wei H (2020) Paleoenvironmental evolution in the Guadalupian (Permian) Gufeng Formation in Chaohu area, Anhui. *Geoscience* 34(1):1–11 (in Chinese)
- Tocqué E, Behar F, Budzinski H, Lorant F (2005) Carbon isotopic balance of kerogen pyrolysis effluents in a closed system. *Org Geochem* 36:893–905
- Veevers JJ, Powell CM (1987) Late Paleozoic glacial episodes in Gondwanaland reflected in transgressive-regressive depositional sequences in Euramerica. *Geol Soc Am Bull* 98:475–487
- Wakeham SG, Lee C (2019) Limits of our knowledge, part 2: selected frontiers in marine organic biogeochemistry. *Mar Chem* 212:16–46
- Wang W, Cao C, Wang Y (2004) The carbon isotope excursion on GSSP candidate section of Lopingian-Guadalupian boundary. *Earth Planet Sci Lett* 220:57–67

- Ward PD, Botha J, Buick R, De Kock MQ, Erwin DH, Garrison GH, Kirschvink JL, Smith R (2005) Abrupt and gradual extinction among Late Permian land vertebrates in the Karoo Basin, South Africa. *Science* 307:709–714
- Wei H, Wei X, Qiu Z, Song H, Shi G (2016) Redox conditions across the G–L boundary in South China: evidence from pyrite morphology and sulfur isotopic compositions. *Chem Geol* 440:1–14
- Wei H, Tang Z, Yan D, Wang J, Roberts AP (2019) Guadalupian (Middle Permian) ocean redox evolution in South China and its implications for mass extinction. *Chem Geol* 530:119318
- Wignall PB, Sun Y, Bond DPG, Izon G, Newton RJ, Védrine S, Widdowson M, Ali JR, Lai X, Jiang H, Cope H, Bottrell SH (2009) Volcanism, mass extinction, and carbon isotope fluctuations in the Middle Permian of China. *Science* 324:1179–1182
- Wu H, Zou D, Gao K (2008) Impacts of increased atmospheric CO₂ concentration on photosynthesis and growth of micro- and macro-algae. *Sci China Ser C Life Sci* 51:1144–1150
- Wu Q, Ramezani J, Zhang H, Wang T, Yuan D, Mu L, Zhang Y, Li X, Shen SZ (2017) Calibrating the Guadalupian Series (Middle Permian) of South China. *Palaeogeogr Palaeoclimatol Palaeoecol* 466:361–372
- Zhang G, Zhang X, Li D, Farquhar J, Shen S, Chen X, Shen Y (2015) Widespread shoaling of sulfidic waters linked to the end-Guadalupian (Permian) mass extinction. *Geology* 43:1091–1094
- Zhang B, Yao S, Hu W, Ding H, Liu B, Ren Y (2019) Development of a high-productivity and anoxic-euxinic condition during the late Guadalupian in the Lower Yangtze region: implications for the mid-Capitanian extinction event. *Palaeogeogr Palaeoclimatol Palaeoecol* 531(part B):108630. <https://doi.org/10.1016/j.palaeo.2018.01.021> (in press)
- Zhang B, Yao S, Mills BJW, Wignall PB, Hu W, Liu B, Ren Y, Li L, Shi G (2020) Middle Permian organic carbon isotope stratigraphy and the origin of the Kamura Event. *Gondwana Res* 79:217–232